Chemistry and Physics of Lipids 218 (2019) 112–124

Contents lists available at ScienceDirect

Chemistry and Physics of Lipids

journal homepage: www.elsevier.com/locate/chemphyslip

Dissecting the thermodynamic contributions of the charged residues in the membrane anchoring of Bcl-xl C-terminal domain

Atanu Maity[1], Souvik Sinha[1], Shubhra Ghosh Dastidar*

Division of Bioinformatics, Bose Institute, P-1/12 C.I.T. Scheme VII M, Kolkata, 700054, India

ARTICLE INFO

Keywords:
Bcl-xl
Membrane insertion
Molecular dynamics
Adaptive biasing force
Potential of mean force

ABSTRACT

The C-terminal helix of the Bcl-xl is known to initiate the membrane insertion of the protein by anchoring into the mitochondrial outer membrane. The C-terminal charged residues of that helix, R232 and K233, are reported to have an important structural role in the process of that insertion. The present work provides a quantitative understanding of the thermodynamic contribution of these residues on the membrane insertion energy-profile, calculated from the Adaptive Biasing Force based MD simulations of 2.67 μs altogether. Interestingly, the effect of the single neutralizing mutations at the C-terminus, i.e. K233A or R232A, is easily tolerated by the peptide without impacting the nature of insertion energy-profile, indicating the efficiency of one positively charged residue to drive the insertion. Whereas a double mutant, i.e. R232A and K233A, makes a significant impact on the energy-profile by destabilizing the membrane-associated states, as well as the membrane-embedded states. The finding provides molecular-level mechanistic insight. The water-mediated interaction formed by the peptide polar side chains within the bilayer core is found to modulate the membrane response during peptide insertion and that subsequently regulates the insertion mechanism. Mutation of the C-terminal residues eventually alters such a cascade of interactions that results in an insertion through energetically more expensive pathway. Since any one of the positively charged residues at the terminal is critical to ensure the membrane insertion, it appears that the natural selection of 'two' instead of 'one' charged residue is redundant in the context of membrane anchoring but may be important for other biochemical events.

1. Introduction

Bcl-2 family of proteins is known to regulate the intrinsic pathway of apoptosis(Brunelle and Letai, 2009). There are two major sub-groups of this family, pro-apoptotic (Bax, Bak) and anti-apoptotic (Bcl-xl, Bcl-2, Bcl-w etc.), whose interplay determines whether apoptosis would be executed or not (Chipuk et al., 2010; Danial, 2007). There is another subgroup that carries death signal arising from different cell stresses to the apoptotic machinery and those are referred as BH3-only proteins (Bim, Bid, Noxaetc) as that share one of the four homology domains (i.e. the BH3 domain) with other Bcl-2 family members. The pro-apoptotic members oligomerize in the mitochondrial outer membrane (MOM) to form proteolipidic pores that allow the release of apoptotic factors (Cytochrome C, Smac/Diablo) followed by a cascade of events leading to apoptosis (Antignani and Youle, 2006; Chipuk et al., 2006). The anti-apoptotic proteins inhibit the process of pore formation either by sequestering the activated pro-apoptotic members through hetero-oligomerization or by antagonizing the death signals carried by the activator BH3-only proteins (Bim, Bid, Noxa etc.) (Billen et al., 2008). As all the activated Bcl-2 family proteins act their cellular function in membrane-embedded population, the role of the membrane is needed to be discussed in the context of differential pathways of action and subsequent functionality of Bcl-2 family members (Kale et al., 2018). The intrinsic pathway of apoptosis is triggered by MOM permeabilization via a cascade of protein-protein or protein-membrane interactions (Leber et al., 2007, 2010). Although there is substantial experimental evidence of structural reorganization of the Bcl-2 family proteins in the membrane-associated state, the molecular details are limited as most experiments did consider fully or partially deleted C-terminal domain (i.e. C-tail) for solubility issue of the protein (Chi et al., 2014).

Abbreviations: MOM, mitochondrial outer membrane; CTWT, C-tail wild type; CTDM, C-terminal double mutant; NTDM, N-terminal double mutant; CTSM, C-terminal single mutant; PMF, potential of mean force; ABF, adaptive biasing force; RC, reaction coordinate; COM, center of mass; MAS, membrane associated states; BP, bulk phase; WMI, water-membrane interface; FI, fully inserted; PE, partially embedded

* Corresponding author.
E-mail address: sgd@jcbose.ac.in (S. Ghosh Dastidar).
[1] Joint first authors.

https://doi.org/10.1016/j.chemphyslip.2018.12.004
Received 9 August 2018; Received in revised form 20 November 2018; Accepted 9 December 2018
Available online 11 December 2018

Fig. 1. Amino acid sequences of the C-tail of four anti-apoptotic Bcl-2 family proteins from *homo sapience*. The residues with charged (red), polar (black) and hydrophobic (green) side chains have been shown with different colors.

Membrane integration of these proteins is generally initiated by anchoring of their putative transmembrane C-tail into the MOM (Hinds et al., 2003; Jeong et al., 2004; Todt et al., 2013) followed by further association of the globular part and consequent structural reorganization. Pro-apoptotic proteins like Bax and Bak perforate the MOM to execute cell death by assembling themselves as oligomer whereas anti-apoptotic Bcl-2 or Bcl-xl integrates to antagonize such process by forming heterodimers with the membrane-embedded pro-apoptotic monomers or by retro-translocating the deathly pro-apoptotic partners out of the MOM. Recent NMR studies of full-length Bcl-xl done in detergent-free lipid nanodiscs have shown that Bcl-xl strongly binds to membrane using its helical C-tail while keeping the BH3-binding groove oriented towards the lipid surface to facilitate binding of exposed BH3 domain of Bax or Bak once those integrates into MOM (Raltchev et al., 2018; Yao et al., 2015, 2016). In a preceding article (Maity et al., 2016),the authors have reported the energy landscape associated with the process of the wild-type Bcl-xl C-tail insertion and corresponding structural changes which were in line with experimental observations (Yao et al., 2016). Further, rigorous structural inspection pointed out that the C-terminal basic residues (Fig. 1) were involved in essential electrostatic interactions with lipid polar head-groups during the insertion event.

Such interactions might have some important energetic contributions to the thermodynamic profile of the peptide insertion into the membrane, yet it was not explored in the previous work. There are experimental reports which suggest that a putative short hydrophobic stretch flanked by basic amino acids is the signature sequence for peptides post-translationally target and insert into MOM (Mihara, 2000; Wattenberg and Lithgow, 2001). Even for Bcl-2 family of proteins (Fig. 1), it has been found that two or more basic amino acid capping at both ends of the hydrophobic transmembrane domain (i.e. the C-tail) are necessary to target MOM specifically, whereas absence of such basic capping is common in endoplasmic reticulum (ER) membrane targeting sequences (Kaufmann et al., 2003). MacCallum et al. compared partitioning of amino acids across the membrane normal and outlined the preference of charged residues (specifically Arg and Lys) around the lipid bilayer head-groups though those can be stabilized even in the bilayer core by causing large water defects (MacCallum et al., 2008). Such preferences can be expected to influence the stability of a naturally occurring transmembrane (TM) peptide at different depth of the bilayer and that's why mutation of such charged residues to neutral ones may revise their course of action. A molecular dynamics based investigation, with all-atom descriptions of the molecular structures and consequent energetics, thus could offer an opportunity to clarify and establish the concerned mechanism. This would be done by quantifying the effect of these mutations on the insertion-thermodynamics which can be helpful to rationalize the experimental observations. The present investigation is planned to shed some light over the energetic impact of the C-terminal single and double mutant on the peptide insertion and how does the membrane respond to such perturbation and optimize its course of action. Findings from the present investigation can serve as a general understanding of the tail-anchored proteins as well as of proteins which share similar kind of sequence at the C-terminal domain, like Bcl-2 family proteins.

2. Materials and methods

2.1. Modeling the membrane-protein assembly

Structure of the wild-type C-tail of Bcl-xl (F210-R233) (referred as CTWT from here onwards) was taken from the earlier work to make the present study consistent with the previous one (Maity et al., 2016). It was modeled using the C-tail of Bax (PDB Id: 1F16) which shares significant sequence similarity with Bcl-xl (Fig. S1). Four mutated systems were then prepared by replacement of amino acids of interest with alanine. The systems are referred as (i) CTDM: CTWT with double mutation (R232A, K233A) at the C-terminal end, (ii) NTDM: CTWT with double mutation (N211A, R212A) at the N-terminal end, (iii) CTSM1: CTWT with single mutation (K233A) at the C-terminal and (iv) CTSM2: CTWT with single mutation (R232A) at the C-terminal. Charged terminals of all the modeled peptides were capped with N-Methylamide (at C-terminal) and acetyl (at N-terminal) groups. The sequence of each system has been mentioned in Table 1.

Equilibrated structure of the DOPC bilayer (80 residues in each layer) was taken from our previous study(Maity et al., 2016). It was modeled using the pre-equilibrated lipid library of CHARMM-GUI membrane builder (Jo et al., 2009). As it is described in the following section, the free energy or the potential of mean force (PMF) profile of peptide insertion into the membrane was computed using the Adaptive Biasing Force (ABF) method (Darve et al., 2008). ABF is a technique that enhances sampling space in a molecular dynamics (MD) simulation and enables computation of the free energy change associated with a

Table 1
Sequence of the variants of C-tail studied. Alanine mutations within the sequence have shown using the underlined bold font.

System Identifier	Description	Sequence
CTWT	C-tail of Bcl-xl	F^{210}NRWFLTGMTVAGVVLLGSLFSRK^{233}
CTDM	CTWT with C-Terminal Double Mutation	F^{210}NRWFLTGMTVAGVVLLGSLFS**AA**^{233}
NTDM	CTWT with N-Terminal Double Mutation	F^{210}**AA**WFLTGMTVAGVVLLGSLFSRK^{233}
CTSM1	CTWT with C-Terminal Single Mutation	F^{210}NRWFLTGMTVAGVVLLGSLFSR**A**^{233}
CTSM2	CTWT with C-Terminal Single Mutation	F^{210}NRWFLTGMTVAGVVLLGSLFS**A** K^{233}

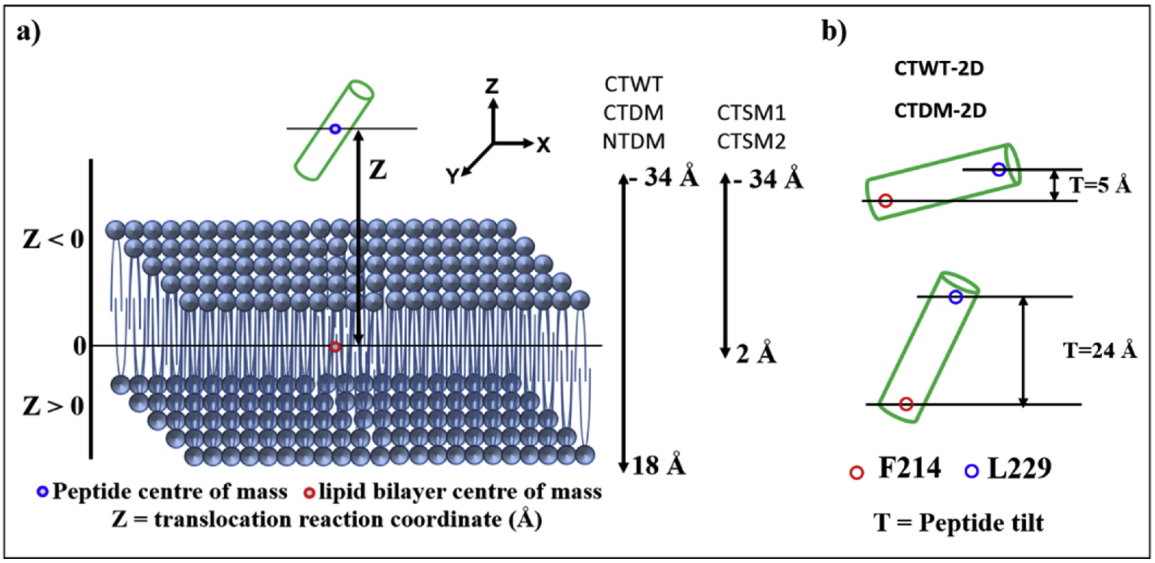

Fig. 2. Definition of the reaction coordinate 'Z' used in the potential of mean force (PMF) calculation, which is the distance between the center of mass (COM) of the membrane (red circle) and COM of the peptide (blue circle) along the membrane normal i. e. z-axis. The PMF profile has been scanned for the range Z = (−34 Å - 18 Å) or Z = (−34 Å - 2 Å) depending on the system as described in the method section.

change of property of interest (i.e. reaction coordinate). For the purpose of better sampling of the reaction coordinate (RC) (discussed in the following section), the entire process is divided into a series of shorter simulations, by compartmentalizing the RC into different windows, which are later integrated to yield the entire profile. For this purpose, the systems were prepared accordingly and in each such said window, the initial position of the peptide differed by 2 Å along the bilayer Z-axis, keeping the membrane position unchanged. It results in a series of separate systems which can describe the step by step translation of the peptide from solvent to the membrane. For each of the CTWT, CTDM and NTDM systems, 26 such windows were prepared, whereas, for CTSM1 and CTSM2, 18 windows were prepared. All the windows were then solvated using a box of size 96 Å x 96 Å x 160 Å containing TIP3P water molecules. Potassium (K^+) and chloride (Cl^-) ions were added, as required, to ensure the overall electrostatic neutrality of the system and then to maintain 0.15 (M) ionic concentration.

2.2. Molecular dynamics simulation and free energy calculations

Peptide partitioning into membrane bilayer would require micro-second order of sampling using equilibrium MD simulation to witness significant conformational change due to the fact that distribution of peptide between the solvent and the membrane-embedded population is separated by a high energy barrier. To overcome this, there are well established sampling enhancement methods (umbrella sampling (Torrie and Valleau, 1977), ABF method (Darve and Pohorille, 2001), meta-dynamics (Laio and Parrinello, 2002) etc.) which offer sampling across energy barriers many fold faster than what it could have been in equilibrium MD simulation. These also help to extract the free energy profile of the process along the RC of interest (i.e. along which the sampling needs to be sufficient). In this work, the ABF method has been employed to compute the free energy landscape of the process of peptide insertion into membrane bilayer from aqueous solvent and systems are prepared accordingly as described in section *2.1*. Before performing ABF simulations, each of such windows was minimized to remove unrealistic steric collisions, using CHARMM package (Brooks et al., 2009). System equilibration and subsequent ABF simulations were carried out using NAMD 2.10 (Phillips et al., 2005). For all these simulations, CHARMM all36 force field and parameter set were used (Best et al., 2012) (Klauda et al., 2010). After minimization, each system was heated to 300 K and then was equilibrated for 5 ns under NVT and NPT conditions respectively. During equilibrations, harmonic restraints were applied to both the peptide and lipid atoms to gradually relax the system where the degree of restraints were reduced slowly to zero in five consecutive equilibration steps. All MD simulations were done at 300 K using Langevin Dynamics with a damping coefficient of 1/ps. The pressure was maintained at 1 atm using the Langevin piston method (Feller et al., 1995) with a coupling constant of τ_p = 0.5 ps. All the bonds involving hydrogen atom were constrained using the SHAKE algorithm (Ryckaert et al., 1977) and 2 fs integration time step was used consequently. To consider a pair of atoms for non-bonded interaction calculation, 16 Å distance criteria was considered and the van der Waals interaction was gradually switched to zero between 12 Å – 14 Å whereas short-range electrostatic was considered up to 14 Å. The long-range electrostatic interactions were calculated using the PME method (Darden and Pedersen, 1993).

The ABF algorithm is implemented in the Collective Variable module (Fiorin et al., 2013) of NAMD. As a general principle, a history-dependent biasing force is applied during the production dynamics to cancel out the instantaneous force and facilitate the sampling along the entire range of reaction coordinate; i.e. for each specific window, sufficient sampling is ensured within the predefined window width (2 Å in the present study) by yielding a reaction coordinate with zero average force acting along it. This biasing is cast adaptively without having any prior knowledge of the PMF and that is the advantage of using this strategy (Comer et al., 2015). The gradient of this force was stored along the chosen collective variable (i.e. reaction coordinate), which was further integrated to get the free energy landscape. ABF method modifies the potential function V(**x**) (**x:** position of the particle) to flatten the energy landscape along described RC (ξ(**x**)) (along which the transition is monitored). During simulation, V changes as V(**x**) –W_t[ξ(**x**)] where W_t[ξ(**x**)] is the potential along the defined RC at time 't' which gets updated in such a way that it converges to the free energy W(Z), defined by-

$$e^{-\beta W(Z)} = \int e^{\beta V(X)} \delta_{\xi(X)-Z}(dx) \quad (1)$$

where W(Z) is the free energy along Z (RC). The Dirac delta function $\delta_{\xi(x)\text{-}Z}(dX)_{(X)\text{-}z}$ is defined by the subset [**x**, ξ(x) = Z] where $\delta_{\xi(x)\text{-}Z}$ (dx) dZ = d**x**. Here β = $1/k_BT$, where k_B is the Boltzmann constant and T is temperature. In a word, the bias (V(**x**) –W_t[ξ(**x**)]) is flattening the energetic barrier between different conformational states without much

Table 2
Reaction coordinate (Z and T) range for different systems.

System Identifier	Reaction coordinate range		Accumulated sampling
	Z	T	
CTWT	−34 Å to 18 Å		390ns
CTDM	−34 Å to 18 Å		390ns
NTDM	−34 Å to 18 Å		390ns
CTSM1	−34 Å to 2 Å		270ns
CTSM2	−34 Å to 2 Å		270ns
CTWT-2D	−10 Å to −18 Å	5 Å to 24 Å	480ns
CTDM-2D	−10 Å to −18 Å	5 Å to 24 Å	480ns
Total sampling time			2.67 μs

affecting the characteristics of the dynamics (Comer et al., 2015).

The Z-distance between the center of mass (COM) of the protein and the lipid bilayer was chosen as the 'translocation' RC (Z) (Fig. 2a) which has already been reported earlier as a good choice for such a system (Maity et al., 2016). Total length of the RC was 52 Å (-34 < ξ < 18 Å) for CTWT, CTDM and NTDM and 36 Å (-34 < ξ < 2 Å) for CTSM1 and CTSM2 (Fig. 2a). Systems and corresponding RCs are also listed in Table 2.

As the time of convergence is proportional to the square of the length of the RC, the 'translocation' RC (Z) was stratified into windows of size 2 Å (as described in section *2.1*) (Valleau and Card, 1972) and a force constant of 100 kcal/Å^{2}mol was applied to restrict the peptide's dynamics outside the specified window. Instantaneous forces were stored in bins of width 0.1 Å. Prior to applying bias, each window was allowed to run 1000 steps of dynamics and then each of them was simulated for 10 ns with adaptive bias after the initial minimization and 5 ns of equilibration. So, each of the double mutant and wild-type system was run for 390 ns and single mutants for 270 ns each.

Along 'Z' RC, where the peptide crosses the water-membrane interface (Z= -10 Å to -18 Å i.e. 4 windows along translocation (Z) RC as each window was of size 2 Å), a 2D free energy landscape was built considering tilt of the peptide (Peptide Tilt: T) with respect to membrane normal as the second reaction coordinate. This was defined by the distance between F214 and L229 of the peptide projected along Z-axis (Fig.2b). This RC was varied from 5 Å to 24 Å which represents a horizontal (perpendicular to the membrane normal) and a vertical orientation (parallel to the membrane normal) respectively. For the 2D PMF, 4 continuous windows have been considered along 'Z' RC and at each Z-window, 8 non-overlapping windows [5–9 Å, 9 − 11 Å, 11 − 13 Å, 13–15 Å, 15–17 Å, 17–19 Å, 19–21 Å, and 21–24 Å] have been constructed along 'T' RC. So total 32 windows were run for 15 ns each (apart from the initial 5 ns equilibration) to build the 2D PMF, i.e. the cumulative sampling time is 2.67 μs for the entire work (Table 2).

2.3. Trajectory analysis

Analysis of the MD trajectories was done using CHARMM and also using scripts developed in-house. The thickness of the membrane at different points was estimated as the average distance between the head-group phosphorus atom of the upper and lower leaflet belong to the same x–y grid. The values were collected considering grids of length 1 Å in both x and y-direction and averaged over the last five nanoseconds of the simulation windows.

The acyl chain order parameter of lipids is considered as a measure of rigidity in the orderliness of the acyl chains of the lipid molecules arranged in the bilayer. It is considered as the inverse of fluidity. The order parameter was calculated according to the following formula (Vermeer et al., 2007).

$$S_{CH} = \frac{1}{2}(3\cos^2\theta - 1) \quad (2)$$

Where θ is the angle of C–H bond vectors of acyl chain with the membrane normal. The value was calculated separately for each acyl carbons (C2-C18) of DOPC and was averaged over all the lipid molecules as well as over the ensemble of conformations. The graphical figures of molecules were prepared using PyMOL (DeLano, 2002) and VMD (Humphrey et al., 1996).

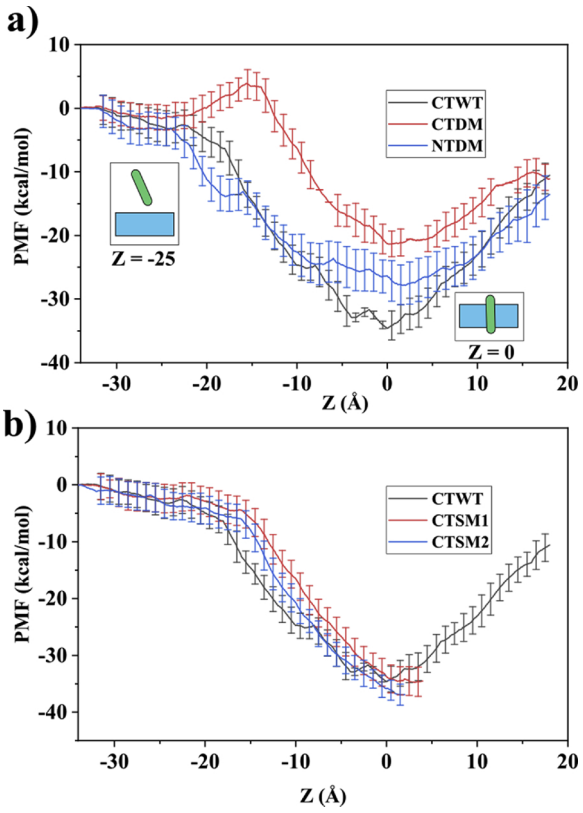

Fig. 3. (a) 1D PMF profiles of insertion of the wild-type C-terminal of Bcl-xl (CTWT) (black) (Maity et al., 2016) and the two double mutants, i.e. CTDM (red), NTDM (blue). The approximate position of the peptide in the membrane is shown using box figures. The CTWT plot has been used here as the reference. (b) Overlay of the PMF of CTWT and the single mutant systems i.e. CTSM1 (red) and CTSM2 (blue). The statistical error of PMF has been added as error bar on each PMF.

3. Results

3.1. Effect of peptide mutation on the membrane-insertion profile

The one-dimensional PMF W(Z), (along the reaction coordinate Z) for wild and mutated systems are compared and presented in Fig. 3. To verify the convergence of the energy profiles as a function of the reaction coordinate, the gradient of free energy was monitored at different stages of the ABF simulations, as the mean force gradually reaches close to zero upon attaining convergence for the range of reaction coordinate considered. An overlay of the gradient of free energy at the beginning of the simulation (1 ns–2 ns) and at the completion of the simulation (9 ns–10 ns) shows that the mean force did converge satisfactorily around zero (Fig.S2). The error (ΔA) has been estimated for the PMF profiles following the equation (Comer et al., 2015)–

$$Err[\Delta A_{a\to b}] = \delta\xi\sqrt{\sum_{i=i_a}^{i_b}\frac{\tau_i}{n_i\Delta t}\langle\Delta F_\xi^2\rangle_i}$$

where, $\langle\Delta F_\xi^2\rangle_i$ is the variance of the random force [i.e. $\Delta F_\xi(\mathbf{x_t}) = F_\xi(\mathbf{x_t}) - \langle F_\xi \rangle_i$] in the i^{th} bin of the reaction coordinate spanning within the range of RC values from a to b; n_i is the number of time the specific bin

(i) has been sampled, Δt is the integration time step and τ_i is the autocorrelation time of system force along the reaction coordinate. On an average, the error was found to be in the range of 3-4 kcal/mol for all the systems.

For CTDM, destabilization of membrane-associated states by ~5 kcal/mol between Z= -20 Å to -15 Å indicates an energetically expensive event of passage through the membrane-water interface (Fig. 3a). Whereas for other systems (Fig. 3a, 3b), membrane-associated states (MAS: peptide in association with the membrane polar head-groups) (Z~ -20 Å to -15 Å) are energetically almost equivalent to the bulk phase (BP: peptide exposed in water) (Z~ -32 Å to -20 Å), which makes the entry of the peptide unconfronted along the 'Z' RC. However, such a situation is unlikely as past studies (MacCallum et al., 2008) have shown that insertion of charged residues into the bilayer core is associated with large energy barriers. It is also possible that presence of many different amino acids in a peptide may compensate each other to offset noticable energy barrier. Yet again, since the conformational space, as well as its free energy landscape, are multidimensional and the reported PMF gives the free energy change along a single dimension ('Z' as the RC), spontaneity of the process along Z does not rule out the possibility of the existence of an energy barrier along any other degree of freedom orthogonal to Z. To investigate such a possibility, an additional RC was chosen (Peptide tilt (T) as described in '*Materials and methods*') along with previously descibed 'Z', to explore the orientation of the peptide with respect to the membrane normal at the water-membrane interface (Z ~ −18 Å to -10 Å along 'Z' RC) and a 2D PMF was built (Fig. 4). Comparison of the 2D PMF at different time point (10 ns, 12 ns, 14 ns and 15 ns) of the 15 ns ABF windows ensures the extent of convergence achieved (Fig. S3 and S4).

Consideration of peptide orientation as the 2nd RC is evident from earlier studies where preference of horizontal orientation at the interfacial state and vertical (or transmembrane orientation) orientation at the bilayer core has been reported in detail (Bond et al., 2008; Chetwynd et al., 2010; Gumbart et al., 2018). As lower value of T (~5-10 Å) represent a horizontal orientation and higher T (~20-24 Å) represent vertical (described in '*Materials and methods*'), both the wild-type (CTWT) and double mutant (CTDM) seem to have reoriented from horizontal to vertical orientation while moving from −18 Å to -10 Å along 'Z' RC which is associated with a substantial energy barrier. At lower T values (~5-8 Å), conformations are mostly stable across the entire range of 'Z' RC considered (more precisely, the CTWT conformations (Fig. 4a) are mostly stable within -18 Å to -14 Å) and at higher T (~20-24 Å), conformations are stable only when peptide is more embedded within the bilayer core (i.e. at lower Z). CTWT conformations (Fig. 4a) were appeared to be stable at higher T over a broader region [Z ~ -14 Å to -10 Å and T ~ 15 Å to 24 Å] of the defined landscape compared to that of the CTDM conformations (Fig. 4b) [Z ~ -12.5 Å to -10 Å and T ~ 17 Å to 24 Å].

The most interesting differences between the two systems lie in the barrier that connects the two minima. Compared to CTWT, the barrier is much steeper for CTDM. The broader maxima for CTWT may be due to availability of flanking polar side chains (R232 and K233) which can access the head-groups even when COM of both the C-terminal residues are placed around the bilayer core (Fig. 4a(i)). For CTDM, the absence of polar residue has made the transition a sharp one (Fig. 4b(i)). A probable minimum free energy path (mfep) (Ensing et al., 2005) has been estimated between two minima separated by barrier while moving from -18 Å to -10 Å along Z **(red** dotted line in Fig. 4). The 2D PMF along mfep has also been projected on 'Z' RC (Fig. S5) and it shows that there isn't much difference in the barrier height (~9–10 kcal/mol) or in position of the barrier along 'Z' RC (Z ~ −13 Å – −11 Å) between CTWT and CTDM. The relatively sharp barrier for CTDM is also evident from this projection. So, what was observed from the 1D PMF, that apart from CTDM all other variants permeate the bilayer spontaneously, is not entirely true as the event under discussion is not one-dimensional at the water-membrane interface. However, after getting the orientation right (i.e. vertical) [Z ~ -12 Å – −11 Å], the peptide is expected to follow the path along 1D RC as the orientation (i.e. vertical) would be maintained until the peptide reaches the other interface.

Position of the global minimum has been appeared to be the same along the 1D RC which is center of the bilayer (Z ~ 0) for all the variants, yet differences found in their stability. For the CTDM and NTDM systems, the energy of respective global minimum has been raised with respect to that of the wild-type by an amount of ~12 kcal/mol and ~5 kcal/mol, respectively (Fig. 3a). On the other hand, the CTSM systems (CTSM1 and CTSM2) are comparable to the wild-type peptide (Fig. 3b), which clearly indicates that only simultaneous mutation of both the C-terminal charged residues makes a notable impact on the thermodynamics of the inserted states instead of a single mutation of either of the two charged residues. Difference in the energy

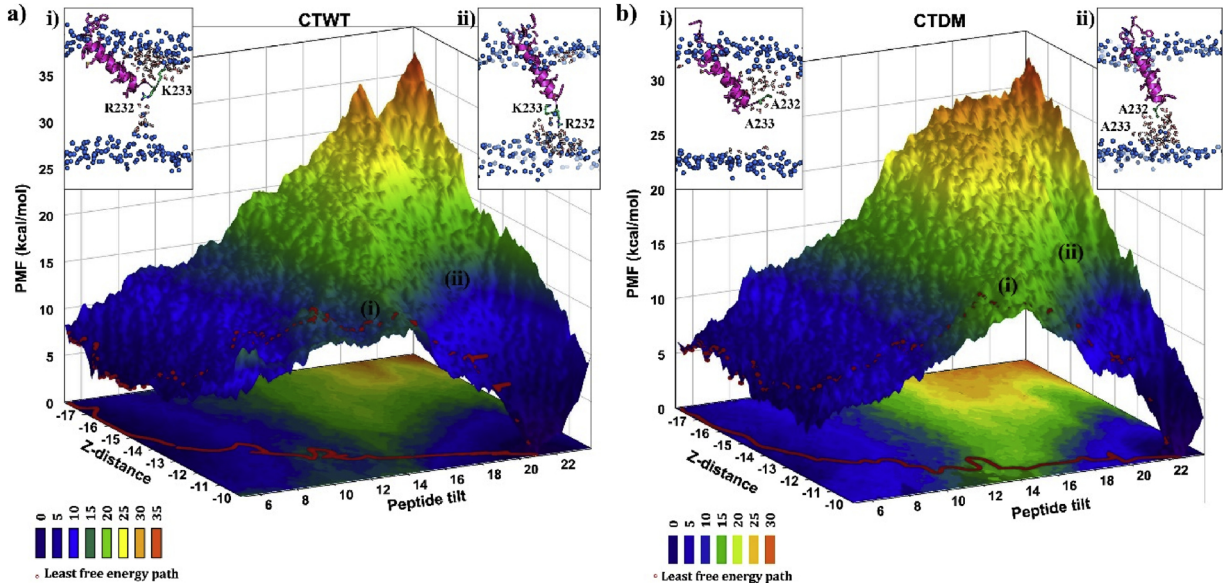

Fig. 4. 2D PMF of (a) CTWT and (b) CTDM insertion considering 'Peptide tilt (T)' as the 2nd RC along with the Z-distance considered for 1D calculation. Blue to red shift in the color scale indicates moving from low energy to high energy region. The red dots on the landscape suggests minimum free energy path (mfep) from one minima to another. Conformations correspond to the specific region of the landscape is shown in inset blocks.

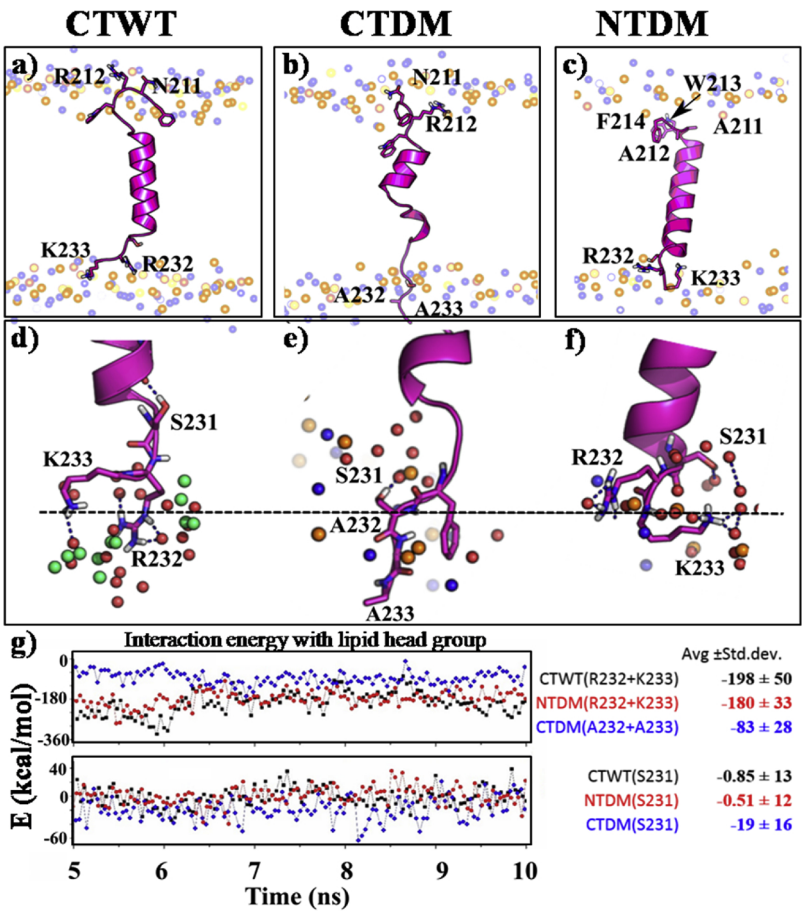

Fig. 5. Conformation and orientation of (a) CTWT, (b) CTDM and (c) NTDM systems at the fully inserted state. Interactions involving CTWT has been reported earlier (Maity et al., 2016). The Phosphorus and nitrogen atoms of the bilayer head-group are shown in sphere representation. The side chains of C-terminal residues and N-terminal residues are shown in the stick representation. (d), (e) and (f) represent the polar interaction between C-terminal end residues and lower lipid head-groups. (g) The interaction energy of R232 and K233 (or Alanine when they are mutated) (upper panel) and S231 (lower panel) with polar atoms of lower lipid head-groups throughout the last 5 ns simulation (the average values with standard deviation have been presented at the right side of the plot).

profiles can be investigated through the change in the interaction of the peptide with the bilayer. The following section characterizes those changes to rationalize the impact.

3.2. Structural detail of membrane-protein interaction

All the peptide variants (wild-type and mutated) are found to be most stable at the center of the bilayer (i. e. at the global minimum along the described RC), which would be referred as 'fully-inserted' (FI) state hereafter. In the FI state, the polar residues (at the terminal ends) were stabilized by polar head-groups of lipid which determined the orientation of the peptide with respect to the bilayer normal. In such orientation (Fig. 5a), the hydrophobic interaction of the peptide with lipid tails add further stability to the FI state of CTWT. Residues N211 and R212 were anchored at the upper lipid head-groups whereas R232 and K233 were anchored to the lower leaflet. Such anchoring helped to maintain the secondary structure of the central hydrophobic stretch (Fig. 5a and Fig.S6a)and mutation of those charged residues eventually altered the scenario.

3.2.1. C-terminal double mutant

Effect of mutation in the FI state is checked by calculating the impact on the interaction energy between residues and lipid polar head-groups. Mutation of C-terminal end residues R232 and K233 to non-polar alanine results in loss of interaction energy with the lower leaflet (~ -83 kcal/mol compared to ~ -198 kcal/mol for CTWT) (Fig. 5b, 5 g). However, the mutated peptide had exposed S231 to the lower leaflet head-group region which caused an increase in the interaction energy with head-group atoms (~ -19 kcal/mol compared to ~ -0.55 kcal/mol for CTWT) (Fig. 5e,5 g). Yet, it failed to recover the secondary structure of the central hydrophobic stretch (Fig. S6b). Exposure of the polar backbone in hydrophobic bilayer core probably did cause an overall destabilization in the PMF of the FI state (~12 kcal/mol) (Fig. 3a) of CTDM compared to that of the CTWT. It is worth mentioning that, direct comparison of interaction energy with the PMF values would be too speculative as different strategies are involved in the calculation of interaction energy (involving single amino acid and the polar atoms (P, N, and O) of the lipid head-group and also not specific along the RC) and in the estimation of PMF, yet the difference is qualitatively comparable in the present scenario as we have considered the same trajectory for both the calculations.

3.2.2. N-terminal double mutant

Upon mutation of the N-terminal end residues N211 and R212, the polar interaction of the peptide with the upper leaflet lipid head-groups was reduced to a large extent, but surprisingly the peptide was found to maintain the orientation with respect to the membrane normal. One reason could have been intercalation of aromatic residues W213 and F214 in between the lipid acyl chains and locking the peptide orientation (Fig. 5c). Intercalation of the aromatic residues has been quantified using the probability distribution of dot products of two vectors (one is parallel to the membrane normal and the other one is perpendicular to the aromatic plane) [Fig S7and SI text]. Anchoring of the C-terminal end in the lower leaflet head-group and exposure of the hydrophobic stretch in the bilayer center (Fig. 5c) could have been other reasons that aids such orientation as well. This vertical orientation may have some help in maintaining the helical structure of the peptide (Fig. S6). Anchoring by the C-terminal end residues is reflected in the interaction energy of S231, R232, and K233 with the lipid head-group region (Fig. 5g) which is consistent with that of the CTWT system.

Table 3
Reaction coordinate (Z) values of the windows.

System Identifier	W1	W2	W3	W4
CTWT, NTDM	−28 Å to -26 Å	−26 Å to -24 Å	−24 Å to -22 Å	−22 Å to -20 Å
CTDM	−22 Å to -20 Å	−20 Å to −18 Å	−18 Å to -16 Å	−16 Å to -14 Å

3.2.3. C-terminal single mutants

To check the impact of the single mutation on the insertion profile, both the C-terminal polar residues have been mutated separately and it was observed that the effect of single mutation at the C-tail was not as destabilizing as in the CTDM system. Such mutation didn't even hamper the vertical orientation of the FI state (Fig. S8) so that the remaining polar residues at the terminal can comfortably be stabilized by the polar interactions with the head-group atoms. At this end, one of the two residues seems to be redundant in the context of insertion followed by stability within the bilayer core.

3.3. Effect of mutation during insertion

Although the 1D PMF did not consider the possibility of different orientation of the peptide around the water-membrane interface (WMI), it certainly did not restrain any probable orientation. Still, it is worth mentioning that the peptide can not freely orient much from its starting conformation (i.e. vertical) itself around WMI along 1D RC. Knowing the effect of the membrane on the partially embedded peptide structures from 1D windows would be useful to understand how the peptide deals with the change of polarity around WMI. For that, 4 consecutive windows (W1-W4) were chosen to scrutinize the impact of the change of environment on the peptide-lipid interaction during insertion. The range of RC values considered for elaboration was different for different systems due to the nature of the energy profile and are listed in Table 3.

3.3.1. Change in peptide conformation around water-membrane interface

To investigate the change in peptide secondary structure during insertion, conformations from the last 5 ns of the ABF windows were considered. In 'W2′ of CTWT, part of the helix become unstructured in an attempt to place the C-terminal polar residues at the upper leaflet head-group (Fig. 6a(iii)) in comparison to the complete helical conformation in 'W1′ (Fig. 6a(ii)). Along the translational axis, some of the previously unstructured domain of the central hydrophobic region (L215 - V224) gets refolded to helix in 'W3′ (Fig. 6a(iv)) when the polar side chains stretch towards the lower leaflet head-groups. The peptide amino acid stretch then gradually forms two helical fragments in W4. One in the lower end of the central hydrophobic region (G222 – S228) and the other on the water phase above the bilayer (N211 - T216) (Fig. 6a(v)).

Upon mutation to CTDM, the terminal residue-mediated interactions with the lipid head-groups were lost. In absence of such polar anchoring, changes in the secondary structure were expected to be guided towards maximizing the hydrophobic interaction with the hydrophobic lipid tail region and that is what exactly found in 'W2′ [Fig. 6b(iii)]. However, in 'W1′, helical structure (Fig. 6b(ii)) was lost to some extent may be to expose polar backbone to the water-membrane polar interface. In 'W3′ and 'W4′, the N-terminal half (i.e. residues 210–220) of the peptide lost its helicity while helical conformation around C-terminal half (i.e. A221- F230) was intact (Fig. 6b(iv-v)).

In the case of NTDM, the patterns of secondary structure transitions in 'W1′, 'W2′ and 'W4′ were found to be comparable to the CTWT system (Fig. 6c(ii, iii,v)) as expected. In 'W3′, helicity was found to be lost in a relatively larger extent than that of in CTWT (Fig. 6c(iv)). Representative structures for all these windows under investigation is provided in Fig. 7.

3.3.2. Change in membrane thickness

To investigate the effect of peptide conformation on the membrane, the thickness of the bilayer was calculated at specific depths of the membrane. The variation of the thickness was projected on the membrane plane (by convention it is the surface perpendicular to the membrane normal) for the same windows, considered for secondary structure analysis (i.e. W1-W4).

For the system containing CTWT, the thickness was reduced to a minimum in the vicinity of the peptide (Fig. 7a(ii-v)). As peptide was partially inserted, the C-terminal polar side chains interact with lower leaflet polar head-groups that squeezed the bilayer in the vicinity of the peptide (Fig. 7a(iv-v)). Upon mutation of the C-terminal residues, though the extent of lowering of thickness in the vicinity of the peptide was reduced (from ∼10 $Å^2$ to ∼5 $Å^2$), surprisingly a moderate reduction in the thickness (∼ 4 $Å^2$ – 5 $Å^2$) is observed all over the lipid bilayer and this was consistent in almost all the windows (Fig. 7b(ii-v)). In contrast, mutation of the N-terminal residues caused a similar impact on the thickness map as it was in CTWT (Fig. 7c(ii-iv)). Thus the change in membrane thickness during insertion is solely influenced by the conformation of C-terminal end residues.

3.3.3. Change in acyl chain order parameter

The bilayer core has fluid-like property (Papahadjopoulos and Watkins, 1967) and that is maintained by the movement of the hydrophobic lipid tails (Hofsass et al., 2003). Interaction with other biomolecules can modulate this fluidity and thereby can change the membrane properties (Khandelia et al., 2008). The relative rigidity or stiffness of the membrane is efficiently represented by the acyl chain order parameters (M'Baye et al., 2008; Van Blitterswijk et al., 1981). Since the physical property of the membrane has been found to be altered during the insertion, the relative difference in the order parameter has been checked in several depths of insertion and also across different systems. For clarity, order parameters have been calculated separately for the upper and lower leaflets. In Fig. 8, an increase in the value of $-S_{CH}$ (Section *2.3* under *'Materials and methods'*) describes a more ordered state and a decrease signifies disorder.

At three specific depths along the insertion pathway, (i.e. FI state (i.e. Z = 0 Å), and partially embedded (PE) state before (i.e. Z = -17 Å) and after the insertion (i.e. Z = 17 Å)), the order parameters of the upper and the lower leaflet were calculated. It has been found that in the FI state the order parameter values are similar in both the leaflets (Fig. 8(a–c)) for all the three variants whereas in the two PE states (Fig. 8(d–i)), there are notable differences among leaflets.

In the PE states before insertion (Z = -17 Å), the order parameter values ($-S_{CH}$) of the lower leaflet are lower compared to the upper leaflet acyl chains i.e. lower leaflet lipids are more disordered compared to the upper leaflet in response to CTWT peptide (Fig. 8d). Whereas, in response to CTDM, the upper leaflet is relatively more disordered in the range C10 – C17 (where CN is the Nth carbon of acyl chain and the DOPC lipid is 18 carbon long) (Fig. 8e) compared to the lower leaflet. So, the mutation didn't let the peptide interact with the lower leaflet at Z = -17 Å due to the absence of anchoring at the lower leaflet. As mutation at the N-terminal (NTDM system) did not affect the peptide-lipid interaction at the discussed depth, the order parameter values are comparable with the wild-type (Fig. 8f).

In the PE state after insertion (i.e. Z = 17 Å), the order parameter values ($-S_{CH}$) of the upper leaflet are lower than that of the lower leaflet

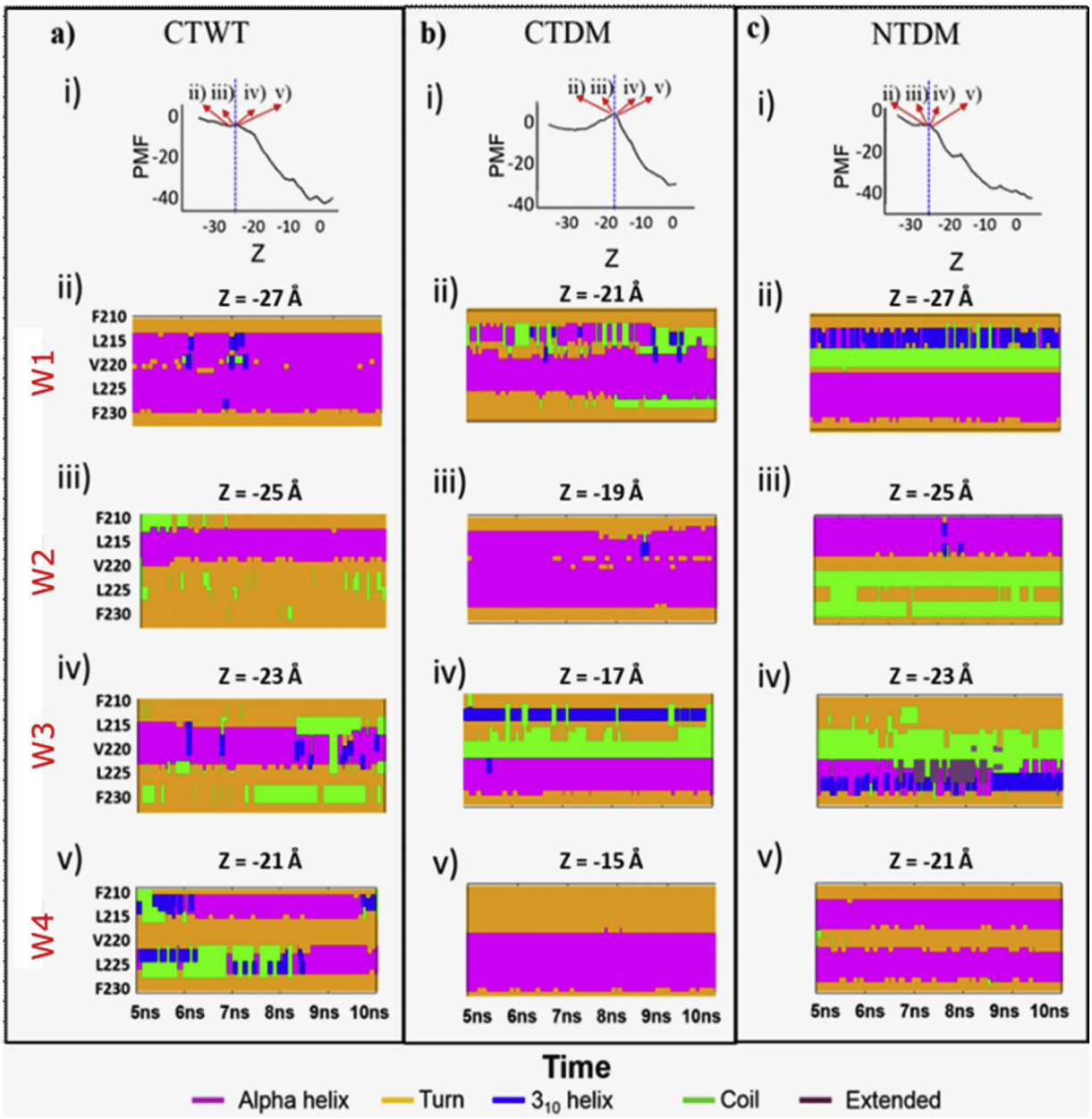

Fig. 6. Evolution of secondary structure of the peptide during the last 5 ns of simulations. Four windows around the water-membrane interface are shown for (a) CTWT, (b) CTDM and (c) NTDM systems. Secondary structure correspond to CTWT windows has been reported earlier (Maity et al., 2016). In the uppermost panel [i], position of the windows has been marked by red arrows on the energy profile and in the subsequent four panel [ii – v], change in secondary structure in the respective windows are presented. The color code describing different secondary structure has been described at the bottom of the plot.

lipids (Fig. 8g), which means that due to interaction with the peptide (CTWT), the upper leaflet of lipid becomes more disordered compared to that of the lower leaflet. In the CTDM system, the overall trend of the order parameter did obviously follow the trend of CTWT (Fig. 8h). Upon mutation of the N-terminal residues (NTDM system), the disorder in the upper leaflet has been reduced to a considerable extent compared to CTWT and CTDM (Fig. 8i).

3.3.4. Alteration in the water assisted interaction between peptide and lipid

In a preceding article, the role of water molecules in maintaining the structural assembly of Bcl-xl C-tail was reported (Maity et al., 2016). The observations were in agreement with the fact that biologically active membranes are found to contain water molecules naturally at different layers inside the bilayer that helps in transportation of important molecules across the bilayer (Leverson et al., 2015). It has also been reported that solvation of the hydrophobic core helped in lowering the insertion free energy of highly charged peptides into zwitterionic bilayers (Herce and Garcia, 2007). Therefore, the analysis of the dynamics of water molecules is importnat for the present investigation. To to that, the water density was calculated along the membrane normal. A plot of water density v/s Z-distance along membrane normal (referred as ZM) (Fig. 9) shows significant variation in density profile upon mutation of the wild-type system for both the fully inserted (FI) state (Z = 0 Å) and the partially embedded state before insertion (Z = -17 Å).

During insertion of the wild-type peptide (CTWT), polar terminal side chains (R323 and K233) were elongated to the lower leaflet aqbilayer interface (Fig. 9g) and subsequently solvate the hydrophobic region to be stabilized in the non-polar bilayer core at the partially inserted states compared to the fully inserted state (Fig. 9a) as described

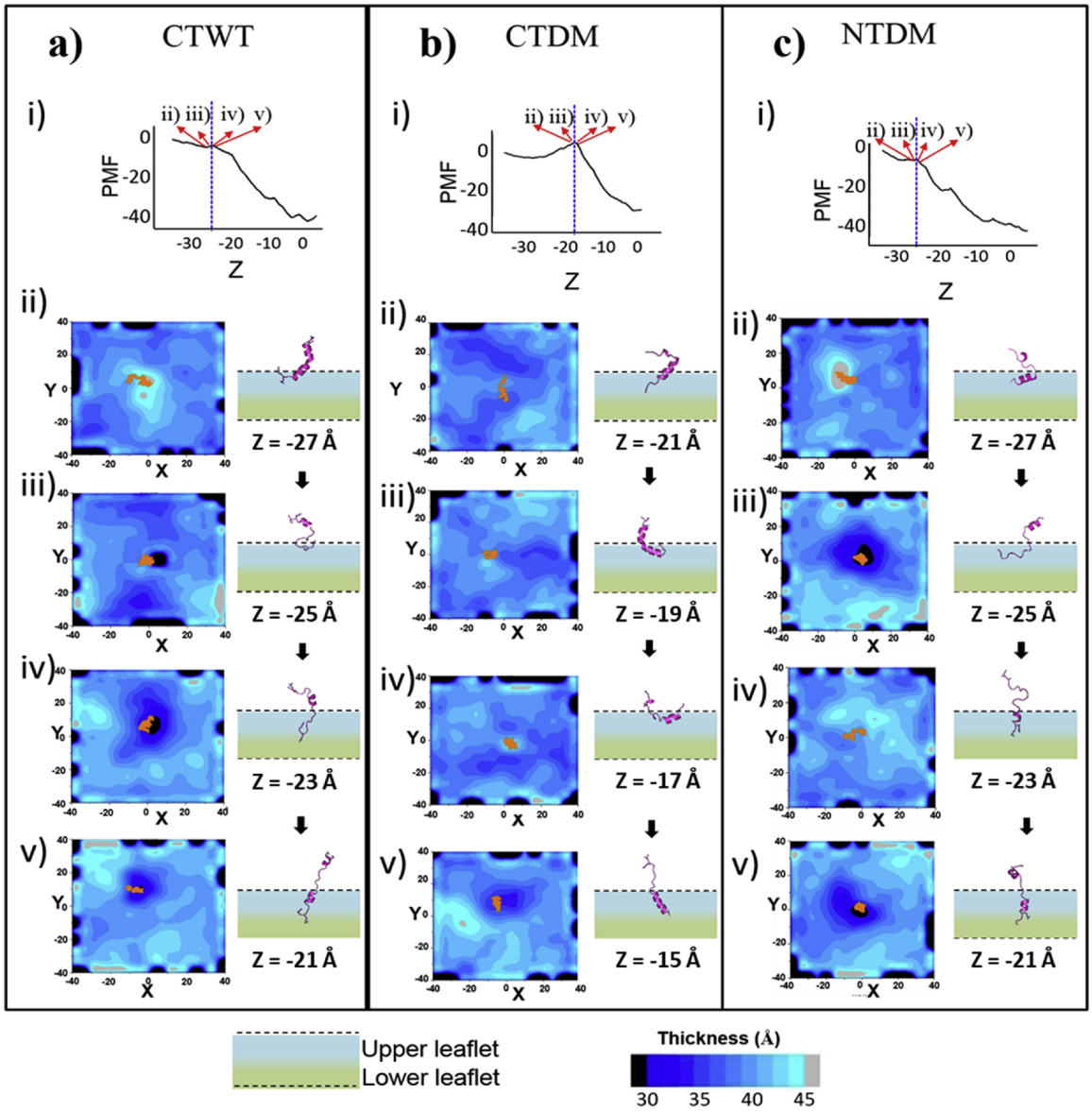

Fig. 7. Average membrane thickness during the last 5 ns of the simulations. Four windows around the water-membrane interface for CTWT, CTDM and NTDM have been shown in panel (a), (b) and (c) respectively. Panels (i–v) followed the same convention as in Fig. 6. Panel (ii - v) describe the thickness on the horizontal (XY) plane (considering membrane normal to be along Z-axis) as a contour changing from **blue** (thinner) to cyan (thicker). Position of the peptide on the horizontal plane (XY plane) during the simulation has been shown using **orange** dots. A representative structure of the peptide for each window has been shown in blocks at the right side of each contour.

in the previous report (Maity et al., 2016). Such stabilizing effect by water molecules was referred as micro-solvation. Maity et al. previously reported that the water molecules participating in micro-solvation differ in several properties compared to the bulk water. The residence time of water involved in micro-salvation was found to be higher than that of the waters in the vicinity of the lipid head-group region whose residence time was higher than that of the bulk water. Similarly, the decay in rotational correlation function was slower for the micro-solvation associated water molecules compared to the bulk water.

In contrary to the PE states (Z = -17 Å) (Fig. 9g), the requirement of water in the FI state was only in the region around the aq-bilayer interface but not within the hydrophobic core for CTWT (Fig. 9c). The absence of charged residues in the mutated systems affected this distribution. For the FI state (Z = 0 Å), water density is comparable among wild-type and mutated systems (Fig. 9b) whereas for the PE states (Z = -17 Å) it varies from system to system (Fig. 9f). In absence of the C-terminal charged residues (i.e. CTDM), as polar side-chain mediated interactions are no longer possible, more number of water molecules are in demand to stabilize the exposed polar backbone (due to loss of helical structure) and the extended S231 (as described previously) plausibly aided to the cause (Fig. 9h) (higher density at ZM > 0 Å). However, the numbers remain almost similar for the NTDM and CTWT systems (Fig. 9f). Since in the FI states, the peptides are anchored at both upper and lower head-groups, the number of water molecule within hydrophobic core does not vary much (Fig. 9d,9e).

Interestingly, in both the FI and PE states, the water density was similar for CTWT and CTSM systems (CTSM1 and CTSM2) (Fig. 9b, 9f) representing the fact that the presence of one charged residue is sufficient for solvating the bilayer core when required.

4. Discussions

It was reported earlier (Maity et al., 2016) that the CTWT inserts spontaneously into the DOPC bilayer along 'Z' RC as evident from the

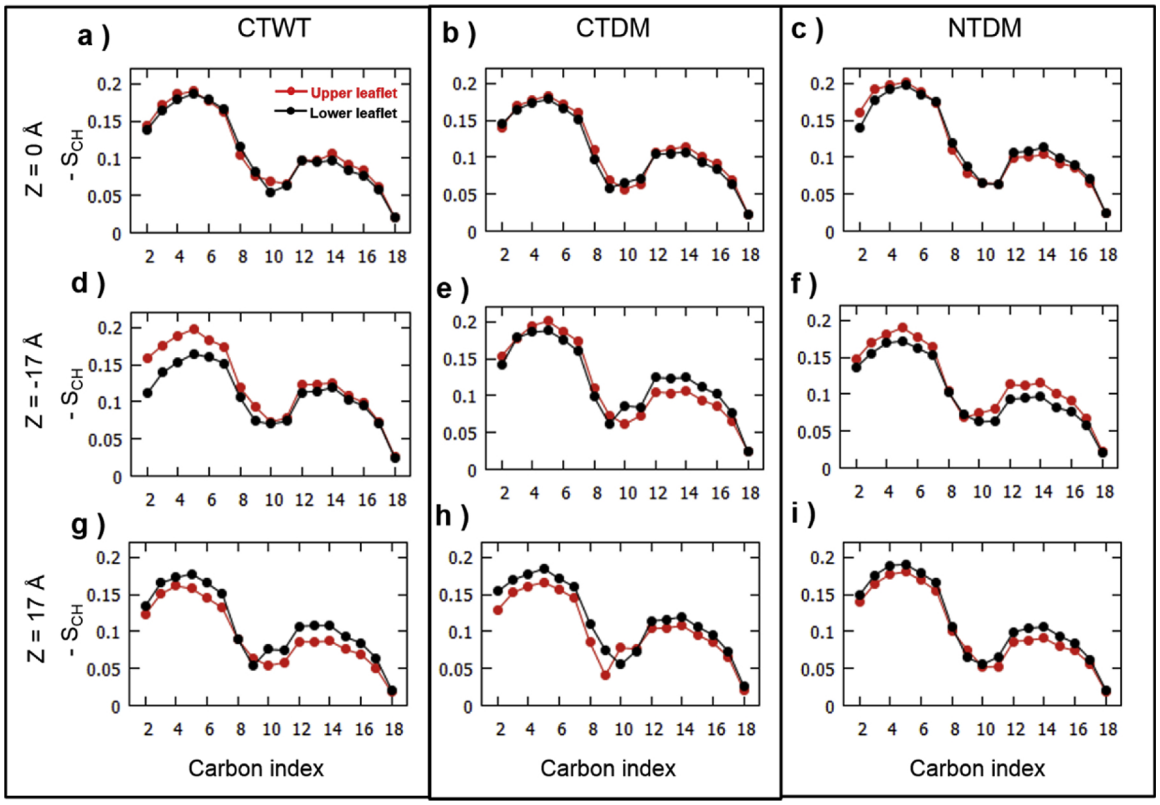

Fig. 8. Acyl chain order parameter ($-S_{CH}$) of lipid bilayer at different positions across the membrane normal. The order parameter of DOPC acyl chain carbons (C2-C18) has been plotted separately for upper (in red) and lower (in black) leaflet. Order parameters at the fully inserted states (Z = 0 Å) are shown in the upper panel, partially inserted states before insertion (Z = -17 Å) in the middle panel and partially embedded states after insertion (Z = 17 Å) in the lower panel. Left panel (a, d, g) represent CTWT, middle panel (b, e, h) for CTDM and extreme right (c, f, i) for NTDM systems.

1D PMF; in that report, the computation of the 2D PMF was done only for the aqueous phase. In the present work, different mutants have been studied to understand the role of terminal polar groups in the insertion mechanism. Along with the 1D PMFs (consistent with the previous study), 2D PMFs have been computed for CTWT and the CTDM in the membrane-associated states, which has provided more detailed insight into the membrane insertion mechanism. Mutation of the C-terminal end charged residues (R232 A and K233 A) has led to the change of specific peptide-lipid interactions that perturbed the bilayer structure and that in turn made an impact on the 1D insertion profile (Fig. 3). Due to such mutations (i.e. CTDM), the fully inserted peptide has failed to benefit from its inclination towards anchoring at the lower leaflet head-groups (Fig. 5). It also cost an effective loss of the helical structure (Fig. S6), which prompted exposure of the polar backbone of the central hydrophobic region to the non-polar bilayer core (Fig. 5b). The combined loss of polar and non-polar stabilization has been reflected in the destabilization of the FI state by ~12 kcal/mol compared to that of the CTWT (Fig. 3). Kaufmann et al. (Kaufmann et al., 2003) suggested a consensus sequence of C-tails (considering exclusively Bcl-2 family of proteins) those targets MOM: $B_{0\text{-}9}B_{0\text{-}2}$-TMD-$B_{0\text{-}1}B_{0\text{-}6}$, where B_n stands for number of basic residues. It was proposed that immediate polar basic residue capping (1–2 residues) around both ends of TMD (transmembrane domain) is the major selector for aiming MOM whereas the second layer (6–9 residues) helps to stabilize the peptide inserted state. Jeong et al. (Jeong et al., 2004) also reported that C-terminal mutants like Δ4C (i.e. truncating 4 residues from the C-terminal end), Δ5C, AAAAA (i.e. C-terminal 5 residues are mutated to Ala) were completely unable to insert into mitochondria isolated from early-stage apoptotic HeLa cells. Other mutants like AAARK, AAAAK, and AAARA were weakly membrane-permeating variants. Though the exact experimented mutants are not considered, the present study is quite in agreement with the experimental findings qualitatively.

The C-tail peptide approaches the membrane bilayer from the aqueous phase by snorkeling its C-terminal Arg and Lys (R232 and K233) side chains to the upper leaflet polar head-groups (Maity et al., 2016). Then it associates and again snorkels the polar side chains to the lower leaflet head-groups during insertion. It resembles stretching of a spring which further pulls rest of the peptide inside. A similar mechanism was also observed for the insertion of the HIV-1 TAT peptide (Herce and Garcia, 2007). Snorkeling ability of Arg and Lys at different depth along bilayer normal to bury their polar side-chains in the head-groups was reported by Johansson and Lindahl (Johansson and Lindahl, 2006) as well. In the case of CTDM, as those polar grips have been replaced by non-polar alanine residues, there is no more an influence of polar interactions to lower the membrane association free energy and that has been implicated by destabilization (~5 kcal/mol) of MAS (-20 Å to -15 Å) in comparison to CTWT (Fig.3a). On the contrary, mutations at the N-terminal end (i.e. NTDM) doesn't disrupt the profile around MAS rather affects only the FI state by an amount of ~5 kcal/mol compared to CTWT, however, it is ~12 kcal/mol in case of CTDM. Here, the insertion process is not influenced much due to the fact that it is primarily guided by the C-terminal end polar residues and therefore, N-terminal mutations do not have any significant role to play unless the peptide is substantially inserted. In the FI state, the absence of N211 and R212 is found to be compensated by the presence of two intercalating aromatic residues W213 and F214 (Fig. S7) for the purpose of anchoring. The aromatic side chains of the amino acids Phe, Trp and Tyr, preferably intercalate into the acyl chains in such a way that the plane of the ring becomes parallel to the plane of membrane normal (Johansson and Lindahl, 2006) and that makes those useful membrane anchor (de Planque et al., 2003). A quantification of the orientations of the aromatic rings has confirmed the preference for the intercalated

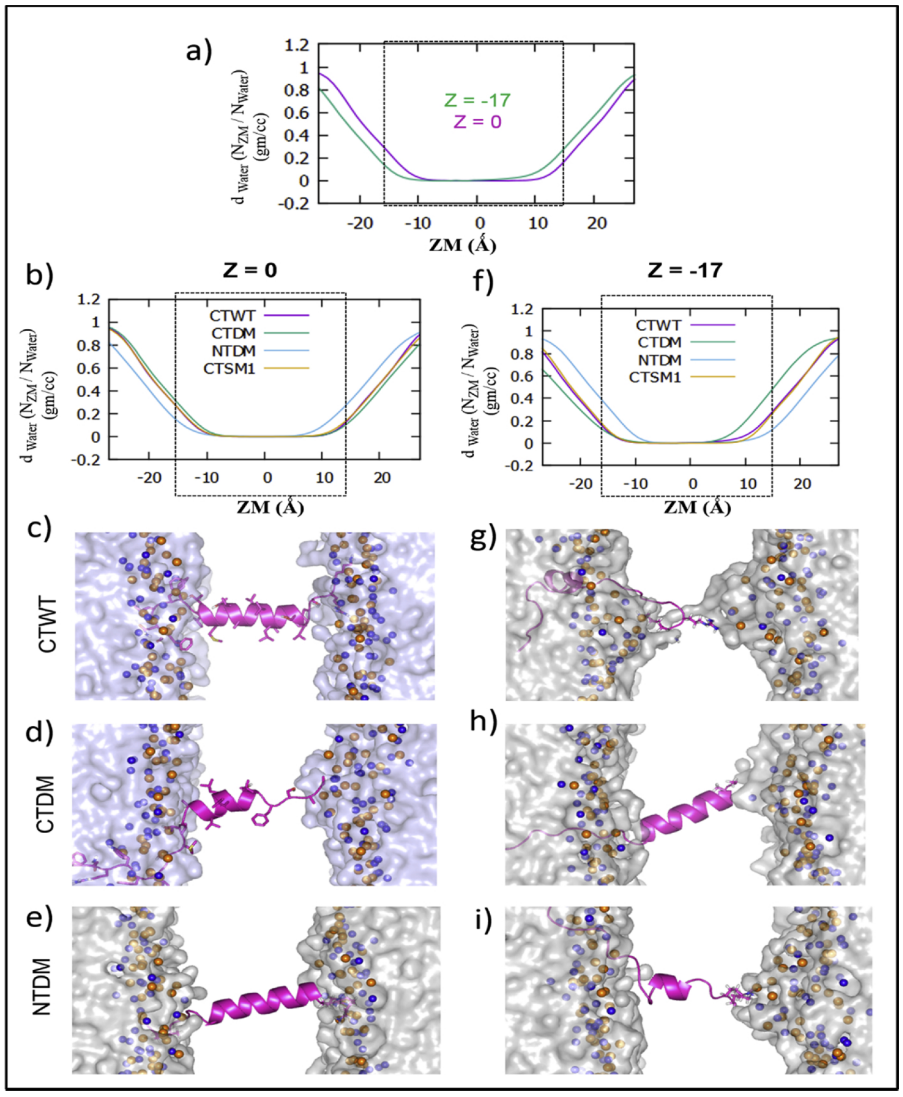

Fig. 9. (a) Difference in water density at the fully (Z = 0 Å) and partially (Z = -17 Å) inserted states for the CTWT. Density (d_{Water}) has been calculated as N_{ZM} / N_{Water} where N_{ZM} is the number of water molecule in the region of bilayer enclosed in the space (ZM – 5) Å to (ZM + 5) Å and N_{Water} is the total number of waters. Comparison among mutated systems at the fully and partially inserted states is shown in (b) and (f) respectively. (c–e) Representative frames of the peptide at the fully inserted state for CTWT, CTDM, and NTDM respectively. Similarly (g–i) represent the partially inserted states in the same order of systems. The Phosphorus and nitrogen atoms of the bilayer headgroup are shown in sphere representation. Water molecules are shown in surface representation. Calculations involving CTWT has been reported earlier (Maity et al., 2016).

orientation in NTDM system [SI text].

The 1D plot along 'Z' RC shows that the entry of the peptide from water to the membrane is barrierless for all other systems except a small barrier for CTDM and thereafter the movement towards the bilayer core is spontaneous. The use of a 2nd reaction coordinate 'T' has allowed the peptide to explore more stable conformations around the water-bilayer interface, which has revealed that horizontal orientation (perpendicular to the bilayer normal) of the peptide is more stable at the interface than that was observed (i.e. vertical) from the 1D PMF. The Fig. 4 and its projection into 1D (Fig S5) suggests that, as states of the peptide outside the membrane are stable and peptide is also stable inside the core of the membrane, these two states are separated by an energy barrier. The 2D PMF (Fig. 4) has also indicated that the peptide has to reorient from the horizontal to vertical orientation with respect to the membrane normal to follow the minimum free energy path (mfep) during insertion and that confronts a barrier of ~ 9–10 kcal/mol (Fig. S5) and the barrier height is almost similar for the CTWT and CTDM. Following the mfep, the barrier height and position of the barrier along 'Z' RC (~ −13 Å – -12 Å) is similar for both CTWT and CTDM, but a major difference lies around the transition point (~ 12 Å – 16 Å) along 'T' RC. Around that region, the 2D landscape is steeper in case of CTDM in comparison to CTWT and that is due to the fact that CTWT can stretch it's two terminal charged side chains (R232 and K233) to both the head group regions at the same time to get hydrated (Fig. 4a(i)) which is not possible for CTDM. Upon mutation, more water penetrates into the core possibly to hydrate the polar backbone to some extent and that eventually induces more disruption in membrane compactness (Fig. 4b(ii)). This may have destabilized subsequent orientations (T ~ 12 Å – 16 Å) to a greater extent for CTDM (Fig. 4b) in comparison to that of CTWT (Fig. 4a). As from the 2D PMF, vertical orientation seems to be more stable than horizontal orientations near the bilayer core Z ~ -10 Å, consequent insertion seems to be spontaneous up to the core (at Z ~ 0 Å) in vertical orientation, which is in full agreement with the previous understanding of the membrane-anchored state of this peptide. Since the relative stabilities of the final state or the fully inserted most stable state of the peptides determine relative probabilities of different peptides to get inserted, the 1D PMF seem to be sufficient for the job. The energy barriers along the path of the insertion only determine the kinetics and do not comment much on the thermodynamic equilibrium. This explains acceptability of the 1D PMF for membrane inserted states and hence the difference in stability of the fully inserted states among different variants. As both CTWT and CTDM provided a 2D landscape of similar nature, such barrier is expected to exist for remaining systems where 1D PMF shows only spontaneous insertion.

Perturbation of the membrane in response to mutations has also been analyzed. In case of CTWT, as the C-terminal polar side chains snorkel to the lower leaflet head-groups during insertion (Z = 17 Å), those take part in polar interactions with the carbonyls and phosphates and also hydrate the local hydrophobic environment (Fig. 9g) by forming H-bonds with water molecules at the lipid-water interface. This

makes the lower leaflet more disordered compared to that of the upper leaflet (Fig. 8d). It also caused local depression in the bilayer thickness around the peptide (Fig. 7a(ii-v)). In contrary to this, due to the absence of flanking polar residues at the C-terminal end, CTDM introduced a bent (Fig. 7b(ii-iii)) or lost helicity (Fig. 6b(iv-v)) to expose its polar backbone to the upper leaflet carbonyls and head-groups and that induced more disorder in that leaflet at Z= -17 Å (Fig. 8e). The unstructured conformation sampled along a larger area of the lipid and caused an overall depression in the membrane thickness [Fig. 7b(ii-v)). Similarly, at Z = 17 Å, when the peptide was leaving the membrane through the lower-leaflet, NTDM perturbed the membrane to lesser extent compared to CTWT (Fig. 8(i)) due to the fact that the mutant is unable to interact with the upper-leaflet head-groups any more. Therefore it can be argued that in the partially embedded states, polar interaction with phosphates and carbonyls of remote leaflets facilitate insertion of the peptide.

It is interesting to notice that the insertion is not bothered much by single mutations of the terminal polar residues. 1D PMF of the CTSM1 and CTSM2 (Fig.3b) resembles the PMF of CTWT. This is because either of R232 or K233 is able to fulfill the structural requirement of polar anchoring in FI state as well as side chain mediated stabilization of the partially embedded states. Fig. S7 shows that upon single mutation of one of the charged residues, the unmutated one serves the purpose of maintaining the orientation and stabilizing the polar interactions.

Kaufmann et al. (Kaufmann et al., 2003) had mutated either of the R232 and K233 with Serine and found that those mutants mostly lost their specificity towards mitochondria-associated localization. Apparently, it seems to be contradicting with our observation. However, it is worth mentioning that our simplified uni-component DOPC bilayer underestimates the effect of negatively charged lipid components (e.g. PG, PI etc.) present in the MOM (Comte et al., 1976). As observing an unbiased 'specificity' of a peptide towards a characteristics bilayer followed by its 'association' and subsequent 'insertion' is computationally rigorous, it is beyond the scope of the present study. However, consideration of negatively charged multi-component lipid bilayer representing MOM may provide more meaningful insights into the membrane insertion mechanism, which is scope for future investigations. In addition, though the present study suggests that any one of the C-terminal charged residues is able to stabilize the membrane-inserted states, the role of both the charged residues in some other functionality like stabilization of the cellular monomeric form (Gomez-Fernandez, 2014; Sinha et al., 2018) cannot be denied as this investigation dealt only with the C-terminal peptide instead of the full-length protein. Not only that, the presence of two or more consecutive terminal charged residues is also known to be common for other tail-anchored proteins those specifically target the mitochondrial outer membrane post-translationally (Borgese et al., 2003; Rapaport, 2003).

5. Conclusion

The C-terminal tail of the Bcl-xl contains charged residues at both ends of the transmembrane domain among which the C-terminal end residues, R232 and K233, play a salient role in the mechanism of insertion. The significance of those charged residues at the terminal end is confirmed by mutating both of them simultaneously, which eventually destabilized the membrane-associated states as well as the fully inserted states. On the contrary, the N-terminal double mutation (N211A and R212A) only decreases the stability of the fully inserted state but has the least impact on the states around the water-membrane interface in comparison to CTDM. The 1D PMF profiles of the wild-type and mutants have been used to compare the stabilities of the peptides in the fully inserted state in the membrane, which in a relative scale reveals the probability of these peptides to get inserted into the membrane. The choice of 2nd reaction coordinate has the role to elucidate the energy barrier that exists in the process of insertion and to find the lowest energy path of the process, although 1D plot along membrane normal is sufficient to show the difference in the probability of insertion of different peptides. After crossing the barrier present along the 2nd reaction coordinate, the wild-type reaches the bilayer core in a vertical orientation by extending its flanking C-terminal side chains to the distant bilayer head-groups and pulling rest of the peptide into the hydrophobic core. This causes only a minimal perturbation to the bilayer in closer proximity of the peptide, which is evident from the discussion of acyl chain order parameters and bilayer thickness. Whereas the C-terminal double mutant (i.e. CTDM) failed to opt a pathway that drives the insertion, rather it leads to perturb the entire bilayer packing causing the insertion a thermodynamically expensive process. On the other hand, single mutation of either of the C-terminal residues (R232A or K233A) does not affect the stability of the membrane-associated states or the membrane-embedded population, which means the absence of one polar residue is compensated by the other. So it can be argued that only one charged residue is able to drive the process of insertion. However, the presence of more charged residues is known to regulate the MOM specific targeting of Bcl-xl and many other tail-anchored proteins those target mitochondrial membrane (Borgese et al., 2003). Another requirement of the two charged residues could be for the stabilization of the cytosolic state where the C-tail binds to the canonical BH3 binding pocket (Gomez-Fernandez, 2014). In a nutshell, the present study provides a detailed atomic insight and thermodynamic assessment of the role of terminal charged residues in peptide partitioning into the membrane.

Conflict of interest

Authors have no conflict of interest to disclose.

Acknowledgments

The work is funded by the project no. BT/PR793/BID/7/370/2011 sanctioned by the Department of Biotechnology (DBT), Government of India. AM thanks 'Center of Excellence' program of DBT (Department of Biotechnology), Government of India, for funds and SS thanks UGC (University Grant Commission), Government of India, for funding. The authors acknowledge M. Moradi (University of Arkansas) for the MFEP code. AM and SS contributed equally.

Appendix A. Supplementary data

Supplementary data associated with this article can be found, in the online version, at https://doi.org/10.1016/j.chemphyslip.2018.12.004.

References

Antignani, A., Youle, R.J., 2006. How do Bax and Bak lead to permeabilization of the outer mitochondrial membrane? Curr. Opin. Cell Biol. 18, 685–689.
Best, R.B., Zhu, X., Shim, J., Lopes, P.E.M., Mittal, J., Feig, M., MacKerell, A.D., 2012. Optimization of the additive CHARMM all-atom protein force field targeting improved sampling of the backbone ϕ, ψ and side-chain χ1 and χ2 dihedral angles. J. Chem. Theory Comput. 8, 3257–3273.
Billen, L.P., Kokoski, C.L., Lovell, J.F., Leber, B., Andrews, D.W., 2008. Bcl-XL inhibits membrane permeabilization by competing with Bax. PLoS Biol. 6, e147.
Bond, P.J., Wee, C.L., Sansom, M.S., 2008. Coarse-grained molecular dynamics simulations of the energetics of helix insertion into a lipid bilayer. Biochemistry 47, 11321–11331.
Borgese, N., Colombo, S., Pedrazzini, E., 2003. The tale of tail-anchored proteins: coming from the cytosol and looking for a membrane. J. Cell Biol. 161, 1013–1019.
Brooks, B.R., Brooks, C.L., Mackerell Jr., A.D., Nilsson, L., Petrella, R.J., Roux, B., Won, Y., Archontis, G., Bartels, C., Boresch, S., Caflisch, A., Caves, L., Cui, Q., Dinner, A.R., Feig, M., Fischer, S., Gao, J., Hodoscek, M., Im, W., Kuczera, K., Lazaridis, T., Ma, J., Ovchinnikov, V., Paci, E., Pastor, R.W., Post, C.B., Pu, J.Z., Schaefer, M., Tidor, B., Venable, R.M., Woodcock, H.L., Wu, X., Yang, W., York, D.M., Karplus, M., 2009. CHARMM: the biomolecular simulation program. J. Comput. Chem. 30, 1545–1614.
Brunelle, J.K., Letai, A., 2009. Control of mitochondrial apoptosis by the Bcl-2 family. J. Cell Sci. 122, 437–441.
Chetwynd, A., Wee, C.L., Hall, B.A., Sansom, M.S., 2010. The energetics of transmembrane helix insertion into a lipid bilayer. Biophys. J. 99, 2534–2540.
Chi, X., Kale, J., Leber, B., Andrews, D.W., 2014. Regulating cell death at, on, and in

membranes. Biochim. Biophys. Acta 1843, 2100–2113.
Chipuk, J.E., Bouchier-Hayes, L., Green, D.R., 2006. Mitochondrial outer membrane permeabilization during apoptosis: the innocent bystander scenario. Cell Death Differ. 13, 1396–1402.
Chipuk, J.E., Moldoveanu, T., Llambi, F., Parsons, M.J., Green, D.R., 2010. The BCL-2 family reunion. Mol. Cell 37, 299–310.
Comer, J., Gumbart, J.C., Henin, J., Lelievre, T., Pohorille, A., Chipot, C., 2015. The adaptive biasing force method: everything you always wanted to know but were afraid to ask. J. Phys. Chem. B 119, 1129–1151.
Comte, J., Maisterrena, B., Gautheron, D.C., 1976. Lipid composition and protein profiles of outer and inner membranes from pig heart mitochondria. Comparison with microsomes. Biochim. Biophys. Acta 419, 271–284.
Danial, N.N., 2007. BCL-2 family proteins: critical checkpoints of apoptotic cell death. Clin. Cancer Res. 13, 7254–7263.
Darden, T.Y., Pedersen, L.G., 1993. Particle mesh Ewald: an N•log(N) method for Ewald sums in large systems. J. Chem. Phys. 98, 10089–10092.
Darve, E., Pohorille, A., 2001. Calculating free energies using average force. J. Chem. Phys. 115, 9169–9183.
Darve, E., Rodriguez-Gomez, D., Pohorille, A., 2008. Adaptive biasing force method for scalar and vector free energy calculations. J. Chem. Phys. 128 144120.
de Planque, M.R., Bonev, B.B., Demmers, J.A., Greathouse, D.V., Koeppe, R.E., Separovic, F., Watts, A., Killian, J.A., 2003. Interfacial anchor properties of tryptophan residues in transmembrane peptides can dominate over hydrophobic matching effects in peptide-lipid interactions. Biochemistry 42, 5341–5348.
DeLano, W.L., 2002. The Pymol Molecular Graphics System. DeLano Scientific, San Carlos, CA USA.
Ensing, B., Laio, A., Parrinello, M., Klein, M.L., 2005. A recipe for the computation of the free energy barrier and the lowest free energy path of concerted reactions. J. Phys. Chem. B 109, 6676–6687.
Feller, S.E.Z., Pastor, R.W., Brooks, B.R., 1995. Constant pressure molecular dynamics simulations: the Langevin piston method. J. Chem. Phys. 103, 4613–4621.
Fiorin, G., Klein, M.L., Henin, J., 2013. Using collective variables to drive molecular dynamics simulations. Mol. Phys. 111, 3345–3362.
Gomez-Fernandez, J.C., 2014. Functions of the C-terminal domains of apoptosis-related proteins of the Bcl-2 family. Chem. Phys. Lipids 183, 77–90.
Gumbart, J.C., Ulmschneider, M.B., Hazel, A., White, S.H., Ulmschneider, J.P., 2018. Computed Free energies of peptide insertion into bilayers are independent of computational method. J. Membr. Biol. 251, 345–356.
Herce, H.D., Garcia, A.E., 2007. Molecular dynamics simulations suggest a mechanism for translocation of the HIV-1 TAT peptide across lipid membranes. Proc. Natl. Acad. Sci. U. S. A. 104, 20805–20810.
Hinds, M.G., Lackmann, M., Skea, G.L., Harrison, P.J., Huang, D.C., Day, C.L., 2003. The structure of Bcl-w reveals a role for the C-terminal residues in modulating biological activity. EMBO J. 22, 1497–1507.
Hofsass, C., Lindahl, E., Edholm, O., 2003. Molecular dynamics simulations of phospholipid bilayers with cholesterol. Biophys. J. 84, 2192–2206.
Humphrey, W., Dalke, A., Schulten, K., 1996. VMD: visual molecular dynamics. J. Mol. Graphics 14 (33–38), 27–38.
Jeong, S.Y., Gaume, B., Lee, Y.J., Hsu, Y.T., Ryu, S.W., Yoon, S.H., Youle, R.J., 2004. Bcl-x (L) sequesters its C-terminal membrane anchor in soluble, cytosolic homodimers. EMBO J. 23, 2146–2155.
Jo, S., Lim, J.B., Klauda, J.B., Im, W., 2009. CHARMM-GUI membrane builder for mixed bilayers and its application to yeast membranes. Biophys. J. 97, 50–58.
Johansson, A.C., Lindahl, E., 2006. Amino-acid solvation structure in transmembrane helices from molecular dynamics simulations. Biophys. J. 91, 4450–4463.
Kale, J., Osterlund, E.J., Andrews, D.W., 2018. BCL-2 family proteins: changing partners in the dance towards death. Cell Death Differ. 25, 65–80.
Kaufmann, T., Schlipf, S., Sanz, J., Neubert, K., Stein, R., Borner, C., 2003. Characterization of the signal that directs Bcl-x(L), but not Bcl-2, to the mitochondrial outer membrane. J. Cell Biol. 160, 53–64.
Khandelia, H., Ipsen, J.H., Mouritsen, O.G., 2008. The impact of peptides on lipid membranes. Biochim. Biophys. Acta 1778, 1528–1536.
Klauda, J.B., Venable, R.M., Freites, J.A., O'Connor, J.W., Tobias, D.J., Mondragon-Ramirez, C., Vorobyov, I., MacKerell Jr., A.D., Pastor, R.W., 2010. Update of the CHARMM all-atom additive force field for lipids: validation on six lipid types. J. Phys. Chem. B 114, 7830–7843.
Laio, A., Parrinello, M., 2002. Escaping free-energy minima. Proc. Natl. Acad. Sci. U. S. A. 99, 12562–12566.
Leber, B., Lin, J., Andrews, D.W., 2007. Embedded together: the life and death consequences of interaction of the Bcl-2 family with membranes. Apoptosis: Int. J. Programmed Cell Death 12, 897–911.
Leber, B., Lin, J., Andrews, D.W., 2010. Still embedded together binding to membranes regulates Bcl-2 protein interactions. Oncogene 29, 5221–5230.
Leverson, J.D., Zhang, H., Chen, J., Tahir, S.K., Phillips, D.C., Xue, J., Nimmer, P., Jin, S., Smith, M., Xiao, Y., Kovar, P., Tanaka, A., Bruncko, M., Sheppard, G.S., Wang, L., Gierke, S., Kategaya, L., Anderson, D.J., Wong, C., Eastham-Anderson, J., Ludlam, M.J., Sampath, D., Fairbrother, W.J., Wertz, I., Rosenberg, S.H., Tse, C., Elmore, S.W., Souers, A.J., 2015. Potent and selective small-molecule MCL-1 inhibitors demonstrate on-target cancer cell killing activity as single agents and in combination with ABT-263 (navitoclax). Cell Death Dis. 6, e1590.
M'Baye, G., Mely, Y., Duportail, G., Klymchenko, A.S., 2008. Liquid ordered and gel phases of lipid bilayers: fluorescent probes reveal close fluidity but different hydration. Biophys. J. 95, 1217–1225.
MacCallum, J.L., Bennett, W.F., Tieleman, D.P., 2008. Distribution of amino acids in a lipid bilayer from computer simulations. Biophys. J. 94, 3393–3404.
Maity, A., Sinh, S., Ganguly, D., Dastidar, S.G., 2016. C-terminal tail insertion of Bcl-x(L) in membrane occurs via partial unfolding and refolding cycle associating microsolvation. Phys. Chem. Chem. Phys. 18, 24095–24105.
Mihara, K., 2000. Targeting and insertion of nuclear-encoded preproteins into the mitochondrial outer membrane. BioEssays: News Rev. Mol. Cell. Develop. Biol. 22, 364–371.
Papahadjopoulos, D., Watkins, J.C., 1967. Phospholipid model membranes. II. Permeability properties of hydrated liquid crystals. Biochim. Biophys. Acta 135, 639–652.
Phillips, J.C., Braun, R., Wang, W., Gumbart, J., Tajkhorshid, E., Villa, E., Chipot, C., Skeel, R.D., Kale, L., Schulten, K., 2005. Scalable molecular dynamics with NAMD. J. Comput. Chem. 26, 1781–1802.
Raltchev, K., Pipercevic, J., Hagn, F., 2018. Production and structural analysis of membrane-anchored proteins in phospholipid nanodiscs. Chemistry 24, 5493–5499.
Rapaport, D., 2003. Finding the right organelle - targeting signals in mitochondrial outer-membrane proteins. EMBO Rep. 4, 948–952.
Ryckaert, J.P., Ciccotti, G., Berendsen, H.J.C., 1977. Numerical integration of the cartesian equations of motion of a system with constraints: molecular dynamics of n-alkanes. J. Comput. Phys 23, 327.
Sinha, S., Maity, A., Ghosh Dastidar, S., 2018. BIM binding remotely regulates BAX activation: insights from the Free energy landscapes. J. Chem. Inf. Model.
Todt, F., Cakir, Z., Reichenbach, F., Youle, R.J., Edlich, F., 2013. The C-terminal helix of Bcl-x(L) mediates Bax retrotranslocation from the mitochondria. Cell Death Differ. 20, 333–342.
Torrie, G.M., Valleau, J.P., 1977. Nonphysical sampling distributions in Monte Carlo free-energy estimation: umbrella sampling. J. Comput. Phys. 23, 187–199.
Valleau, J., Card, D., 1972. Monte Carlo estimation of the free energy by multistage sampling. J. Chem. Phys. 57, 5457–5462.
Van Blitterswijk, W.J., Van Hoeven, R.P., Van der Meer, B.W., 1981. Lipid structural order parameters (reciprocal of fluidity) in biomembranes derived from steady-state fluorescence polarization measurements. Biochim. Biophys. Acta 644, 323–332.
Vermeer, L.S., de Groot, B.L., Reat, V., Milon, A., Czaplicki, J., 2007. Acyl chain order parameter profiles in phospholipid bilayers: computation from molecular dynamics simulations and comparison with H-2 NMR experiments. Eur. Biophys. J. Biophys. 36, 919–931.
Wattenberg, B., Lithgow, T., 2001. Targeting of C-terminal (tail)-anchored proteins: understanding how cytoplasmic activities are anchored to intracellular membranes. Traffic 2, 66–71.
Yao, Y., Fujimoto, L.M., Hirshman, N., Bobkov, A.A., Antignani, A., Youle, R.J., Marassi, F.M., 2015. Conformation of BCL-XL upon membrane integration. J. Mol. Biol. 427, 2262–2270.
Yao, Y., Nisan, D., Fujimoto, L.M., Antignani, A., Barnes, A., Tjandra, N., Youle, R.J., Marassi, F.M., 2016. Characterization of the membrane-inserted C-terminus of cytoprotective BCL-XL. Protein Expr. Purif. 122, 56–63.